Microstrip Elliptic-Function Low-Pass Filters Using Distributed Elements or Slotted Ground Structure

Wen-Hua Tu, *Student Member, IEEE*, and Kai Chang, *Fellow, IEEE*

***Abstract*—This paper presents two microstrip elliptic-function low-pass filters, one using distributed elements and one using a slotted ground structure. The one using distributed elements consists of a microstrip line section in parallel with an interdigital capacitor; the other one using a slotted ground structure consists of a low-impedance microstrip line with a slotted ground structure cell under the center of the line. A transmission-line model and a full-wave simulation are used to calculate the inductance/capacitance values of the equivalent circuits. The design concept was validated through experiments showing good agreements with the full-wave simulated results.**

***Index Terms*—Elliptic-function filter, interdigital capacitor, low-pass filter, microstrip filter.**

I. Introduction

In MANY communication systems, low-pass filters are the key components to suppress the undesired harmonics and spurious signals. The conventional stepped-impedance filters, however, can only provide a gradual cutoff frequency response [1]. In order to achieve a sharp cutoff frequency response, more sections are needed, but more sections will also increase the insertion loss in the passband and the circuit size. Recently, semilumped low-pass filters [2] have been reported with a sharp cutoff frequency response due to the usage of the lumped capacitors. Unfortunately, soldering lumped components not only introduces parasitics, but also makes manufacturing repeatability difficult to maintain. Low-pass filters using coupled lines [3] or stepped-impedance hairpin resonators [4] have finite attenuation poles in the cutoff frequency band. However, because the capacitance of the coupled lines is too small, the finite attenuation pole cannot be located close to the passband. Consequently, the cutoff frequency response is gradual. The low-pass filter [5] with a microstrip line section and an interdigital capacitor has been proposed for sharp rejection, but the analysis is focused on locating the attenuation poles for suppressing the specific harmonics and spurious signals. Little design information is given for desired filter specifications (e.g., passband ripple, rejection level, and equal-ripple stopband starting frequency for elliptic-function low-pass filters). On the other hand, the low-pass filters using slotted ground structure [6], [7] have been recently reported. However, as mentioned in [7], the filter [6] using open stubs and a high-impedance line occupies a large circuit size. With a wide microstrip line, the filter in [7] eliminates the need for the open stubs and high-impedance lines, but only Chebyshev low-pass filters have been reported, and no elliptic-function low-pass filters have been studied.

In this paper, design methods for microstrip elliptic-function low-pass filters using distributed elements or slotted ground structure are presented. The transmission-line model and full-wave simulation are used to calculate the equivalent *L–C* values of the microstrip line sections, the interdigital capacitor, and the slotted ground structure. Since no lumped component is used, it is easy to fabricate these planar filters. For the filters using an interdigital capacitor, because the interdigital capacitor can provide a bigger parallel capacitance, the finite attenuation pole can be located closer to the passband, thus achieving a sharper cutoff frequency response. The filter using a slotted ground structure has the advantage of easy synthesis for the desired *L–C* values. The design concepts of these two filters are all validated through simulations and measurements with good agreement, as discussed in Sections II and III. The comparison between these filters is outlined in Section IV.

II. Elliptic-Function Low-Pass Filters Using Distributed Elements

For low-frequency filters, discrete lumped elements are used to realize the required *L–C* values. However, for high-frequency filters, not only the soldering, but also the size of the lumped elements that are no longer small in comparison with the wavelength can cause parasitic problems. To eliminate the soldering problems, distributed elements are used in microwave/millimeter-wave bands. By using a simple transmission-line model and full-wave simulation, the equivalent *L–C* values of the distributed elements are calculated within the passbands. Although the desired passband response can be predicted very well, the stopband response is different from that of the discrete ideal lumped-element filter. Therefore, full-wave simulations should be carried out to predict the stopband response. Nevertheless, the required *L–C* values and the calculated *L–C* values of the distributed elements still provide useful design information and help the full-wave optimization.

A. L–C Values Calculation

Fig. 1(a) shows the configuration of the elliptic-function low-pass filter. The filter consists of a microstrip line section in parallel with an interdigital capacitor. Fig. 1(b) shows the equivalent circuit, where L_s is the equivalent inductance of the microstrip line section, C_g is the equivalent series capacitance of the interdigital capacitor, and C_{ps} is the sum of the equivalent

Manuscript received May 3, 2006; revised July 7, 2006.

The authors are with the Department of Electrical and Computer Engineering, Texas A&M University, College Station, TX 77843-3128 USA (e-mail: whtu@tamu.edu; chang@ece.tamu.edu).

Color versions of Figs. 5, 6(c), 6(d), and 9 are available online at http://ieeexplore.ieee.org.

Digital Object Identifier 10.1109/TMTT.2006.882896

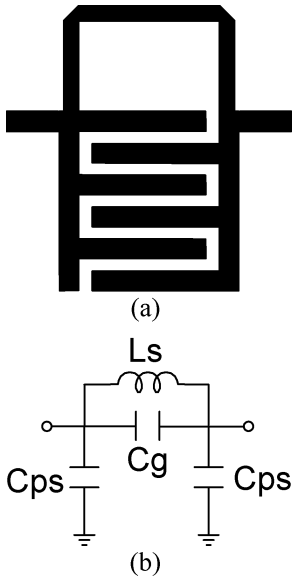

Fig. 1. Microstrip elliptic-function low-pass filter using distributed elements. (a) Schematic. (b) Equivalent-circuit model.

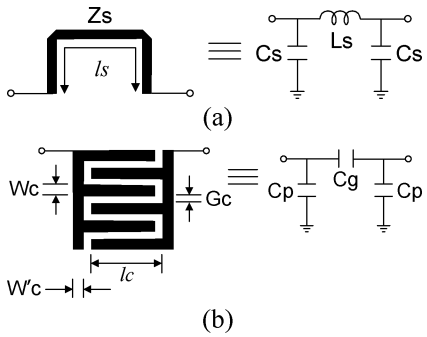

Fig. 2. Schematic and equivalent-circuit model of the: (a) microstrip line section and (b) interdigital capacitor.

shunt capacitances of the microstrip line section and interdigital capacitor. The transmission-line model is used to calculate the equivalent-circuit elements of the microstrip line section. Since the structure of the interdigital capacitor is complicated, parasitic effects should also be considered using a full-wave simulator together with transmission-line model calculation.

Fig. 2(a) shows the schematic and equivalent π-network circuit of the microstrip line section. For a lossless transmission line with the electrical length of θ, the equivalent inductance L_s and capacitance C_s are given by [4]

$$L_s = \frac{Z_s \sin\theta}{\omega} \quad \text{(H)} \tag{1a}$$

and

$$C_s = \frac{1-\cos\theta}{\omega Z_s \sin\theta} \quad \text{(F)} \tag{1b}$$

where Z_s is the characteristic impedance of the transmission line section, and ω is the angular cutoff frequency.

Fig. 2(b) shows the schematic and equivalent π-network circuit of the interdigital capacitor. In order to take all discontinuities into consideration, assuming a lossless and symmetrical

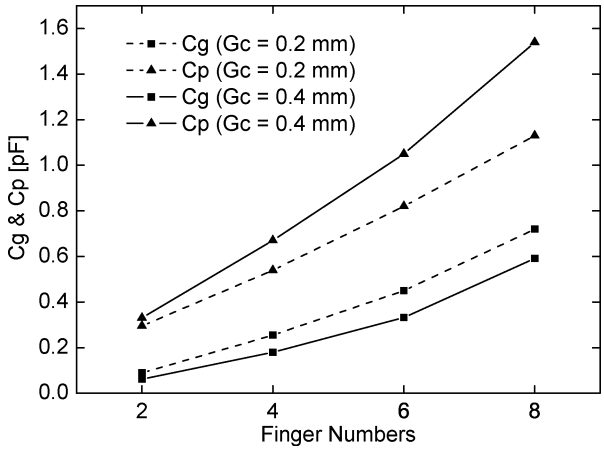

Fig. 3. C_g and C_p values with different finger numbers. Dash line: $G_c = 0.2$ mm, solid line: $G_c = 0.4$ mm.

case, a full-wave electromagnetic simulator [8] is used to calculate the two-port Y-parameters of the specific interdigital capacitor, and then the equivalent capacitances C_g and C_p are given by [9], [10]

$$C_g = -\frac{\mathrm{Im}(Y_{21})}{\omega} \tag{2a}$$

and

$$C_p = \frac{\mathrm{Im}(Y_{11}+Y_{21})}{\omega}. \tag{2b}$$

To gain an insight into the relation between the interdigital capacitor dimensions and capacitance values, many full-wave simulations of different interdigital capacitors were carried out to synthesize the required capacitances. Fig. 3 shows a design figure of C_g and C_p versus finger numbers. The substrate is a 25-mil RT/Duroid 6010.8 substrate with a dielectric constant of 10.8. The dimensions are $W_c = W_c' = 0.3$ mm, $l_c = 2$ mm, $G_c = 0.2$ or 0.4 mm, and finger number $= 2, 4, 6$, and 8. It shows that C_g and C_p increase as finger numbers increases, C_g deceases as G_c increases, while C_p increases as G_c increases due to more metal coverage. Since there are many parameters (W_c, l_c, and G_c) that can be varied, it is easier to realize the required capacitors C_g and C_p in this filter than in a filter using couple lines [4].

B. Implementation of Elliptic-Function Low-Pass Filters

The design procedure of the proposed filter is described here. The prototype elliptic-function low-pass filter element values [9] for $n = 3$, passband ripple $L_{Ar} = 0.1$ dB, and stopband attenuation $L_{As} = 18.86$ dB with the equal-ripple stopband starting normalized frequency $\Omega_s = 1.6949$ are $g_1 = 0.8333$, $g_2 = 0.8439$, $g_2' = 0.3252$, and $g_3 = 0.8333$. The required *L–C* values are calculated by [9]

$$L_{s,\mathrm{Required}} = \frac{Z_0 g_2}{2\pi f_c} = 3.37 \text{ nH} \tag{3a}$$

$$C_{g,\mathrm{Required}} = \frac{g_2'}{Z_0 \times 2\pi f_c} = 0.52 \text{ pF} \tag{3b}$$

$$C_{ps,\mathrm{Required}} = \frac{g_1}{Z_0 \times 2\pi f_c} = 1.33 \text{ pF} \tag{3c}$$

TABLE I
L–C VALUES FOR THE ELLIPTIC-FUNCTION LOW-PASS FILTER

	Cps	Cg	Ls
Required L-C values	1.33 pF	0.52 pF	3.37 nH
Approximately calculated L-C values	1.18 pF	0.45 pF	3.37 nH

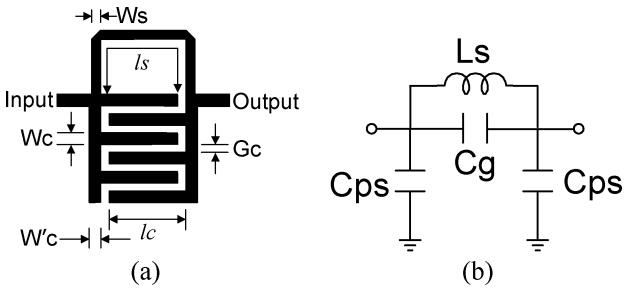

Fig. 4. Elliptic-function low-pass filter using distributed elements. (a) Schematic. (b) Equivalent-circuit model. ($C_{ps} = C_p + C_s$).

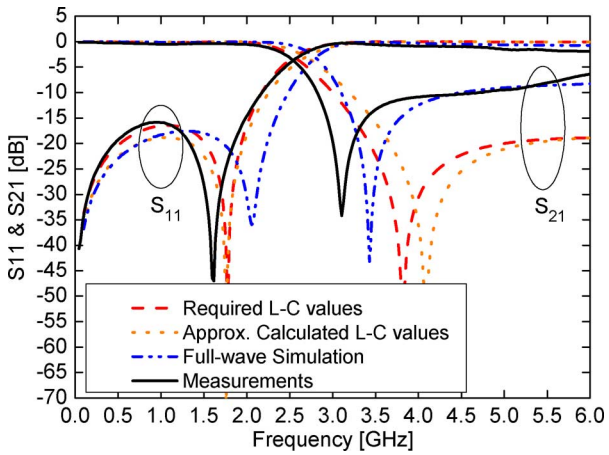

Fig. 5. Simulated and measured results of the low-pass filter using distributed elements.

where the cutoff frequency is $f_c = 2$ GHz, and Z_0 is the source/load impedance of 50 Ω. In order to realize the circuit element $L_s = 3.37$ nH, one can use (1) to calculate Z_s and θ as 72 Ω and 36°, respectively, and consequently, $L_s = 3.37$ nH and $C_s = 0.36$ pF. From Fig. 3, when the finger number $= 6$ and $G_c = 0.2$ mm, it shows that $C_g = 0.45$ pF, $C_p = 0.82$ pF, and then $C_{ps} = C_p // C_s = C_p + C_s = 1.18$ pF, which is close to the required *L–C* values. Table I summarizes the required *L–C* values calculated by (3) and the approximately calculated *L–C* values by (1) and (2).

Fig. 4 shows the schematic of the low-pass filter with $W_s = 0.23$ mm, $l_s = 5.06$ mm, $W_c = W_c' = 0.3$ mm, $G_c = 0.2$ mm, $l_c = 2$ mm, 50-Ω feed linewidth $= 0.57$ mm, and 50-Ω feed line length $= 15$ mm. Fig. 5 shows the simulated and measured results. The full-wave simulation is obtained by IE3D [8], and the results for the required *L–C* values and the approximately calculated *L–C* values are obtained by using AWR Microwave Office. From dc to 2 GHz, the return loss is better than 16 dB and the insertion loss is less than 0.51 dB. An attenuation pole is located at 3.1 GHz. The measured stopband attenuation L_{As} is approximately 10 dB. Measurements agree well with simulations within the passband. There are some minor discrepancies observed due to the fabrication tolerance.

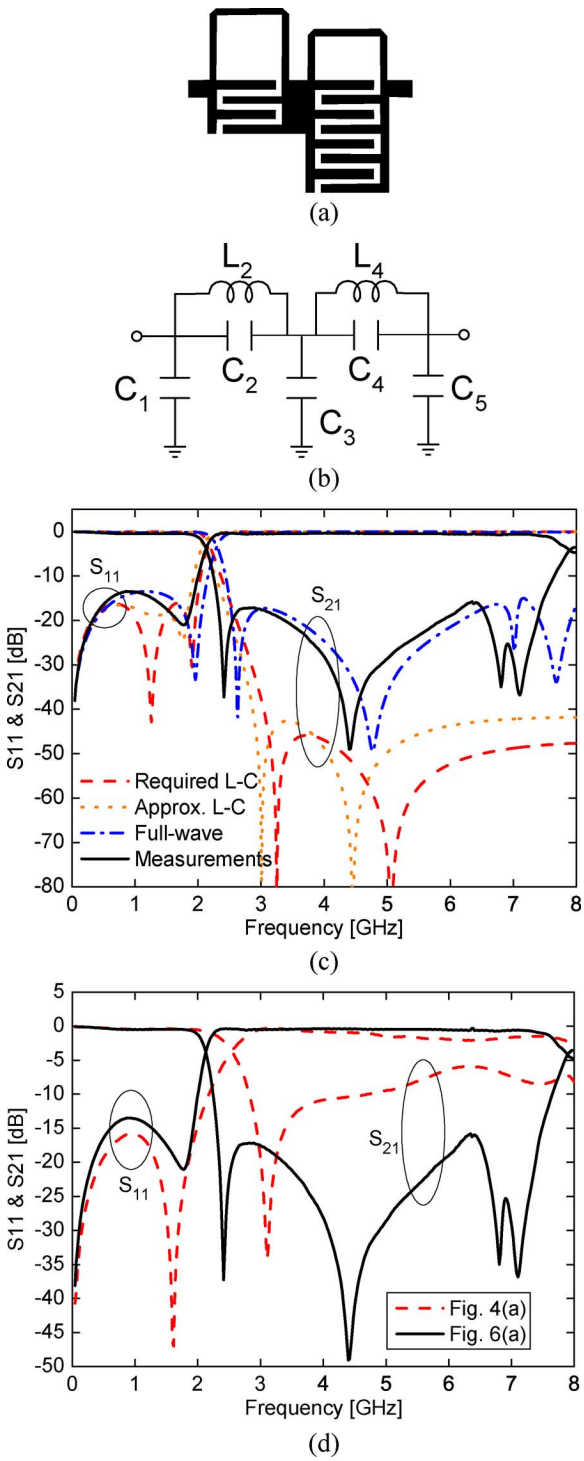

Fig. 6. Two-section low-pass filter. (a) Schematic. (b) Equivalent circuit. (c) Simulated and measured results. (d) Comparison with one-section low-pass filter.

For the stopband response, the full-wave simulation, as expected, agrees better with the measured results when compared to the simulated results of the required *L–C* values and the approximately calculated *L–C* values. This is because the equivalent *L–C* values of the distributed elements are calculated according to the passband characteristics only [11]. In order to increase the stopband rejection, a two-section low-pass filter with different units is designed as shown in Fig. 6(a). The

TABLE II
L–C VALUES FOR THE ELLIPTIC-FUNCTION LOW-PASS FILTER
(UNIT: pF AND nH)

	C_1	C_2	L_2	C_3	C_4	L_4	C_5
Required L-C values	1.7	0.2	4.9	2.7	0.6	4	1.4
Approximately calculated L-C values	1.2	0.26	4.9	2.7	0.7	4	1.6

prototype elliptic-function low-pass filter element values [9] for $n = 5$, passband ripple $L_{Ar} = 0.1$ dB, and stopband attenuation $L_{As} = 47.6$ dB with the equal-ripple stopband starting normalized frequency $\Omega_s = 1.6129$ are $g_1 = 1.0481$, $g_2 = 1.2416$, $g_2' = 0.1244$, $g_3 = 1.6843$, $g_4 = 1.0031$, $g_4' = 0.354$, and $g_5 = 0.8692$. By (3), one can calculate the equivalent *L–C* values shown in Fig. 6(b). They are $C_1 = 1.7$ pF, $C_2 = 0.2$ pF, $L_2 = 4.9$ nH, $C_3 = 2.7$ pF, $C_4 = 0.6$ pF, $L_4 = 4$ nH, and $C_5 = 1.4$ pF. For $C_2 = 0.2$ pF, by Fig. 3, a four-digit capacitor with $G_C = 0.2$ mm is chosen for $C_g = 0.26$ pF and $C_p = 0.54$ pF. For $L_2 = 4.9$ nH, by (1), a 72-Ω and 59° line is given for $L_s = 4.9$ nH and $C_s = 0.63$ pF. For $C_4 = 0.6$ pF, by Fig. 3, an eight-digit capacitor with $G_C = 0.2$ mm is found for $C_g = 0.72$ pF and $C_p = 1.1$ pF. For $L_4 = 4$ nH, by (1), a 44-Ω and 72° line is chosen for $L_s = 4$ nH and $C_s = 0.45$ pF. Table II summaries the required and approximated *L–C* values. Fig. 6(c) shows the simulated and measured results. The full-wave simulation is obtained by IE3D [8], and the results for the required *L–C* values and the approximately calculated *L–C* values are obtained by using AWR Microwave Office. From dc to 2 GHz, the return loss is better than 14 dB and the insertion loss is less than 0.9 dB. The measured stopband attenuation L_{As} is approximately 15 dB. Simulations agree well with measurements within the passband. There are some minor discrepancies observed due to fabrication tolerances. Fig. 6(d) compares the one- and two-section low-pass filter. The two filters show similar passband response. The two-section filter shows a sharper cutoff frequency response and a deeper stopband rejection.

In summary, the design procedure is outlined as follows.

1) Given the filter specifications $(n, L_{Ar}, L_{As}, \ldots)$, use the available table and determine the element values $(g_1, g_2, \ldots)$.
2) Using (3), calculate the required *L–C* values $(L_s, C_g, \ldots)$.
3) Using (1), choose the impedance (Z_s) and the length of the microstrip line section.
4) Obtain the full-wave simulation results of several interdigital capacitors using IE3D [8], and calculate the equivalent capacitors C_g and C_p using (2).
5) Choose a proper interdigital capacitor such that the approximately calculated *L–C* values from Steps 3) and 4) are closest to the required *L–C* values from Step 2).

III. ELLIPTIC-FUNCTION LOW-PASS FILTER USING SLOTTED GROUND STRUCTURE

Fig. 7 shows the three-pole elliptic-function low-pass filter using a slotted ground structure. The filter consists of a low-impedance microstrip line and a dumbbell slotted ground structure located under the center of the line. The equivalent-circuit

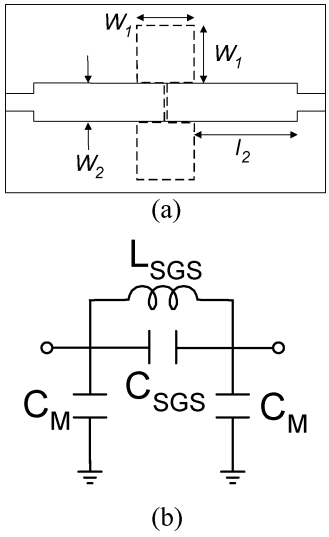

Fig. 7. Elliptic-function low-pass filter using slotted ground structure. (a) Schematic (dashed line shows a dumbbell slotted ground structure). (b) Equivalent-circuit model.

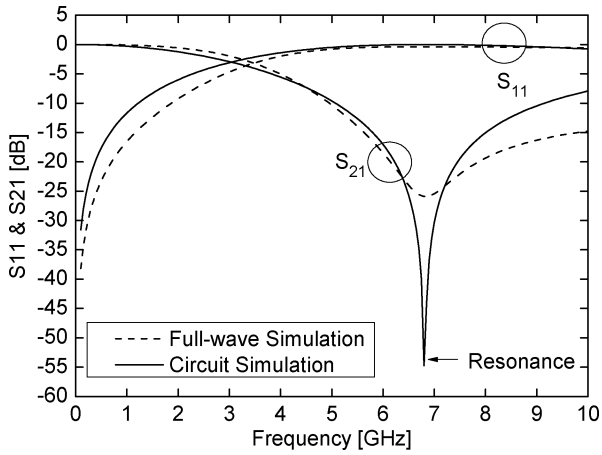

Fig. 8. Simulated results of a slotted ground structure. ($W_1 = 5$ mm, $W_2 = 3.5$ mm width of thin slot $= 0.2$ mm, and length of thin slot $= 3.5$ mm.)

model for the slotted ground structure is a parallel $L_{\rm SGS} - C_{\rm SGS}$ tank [6], [7], where $L_{\rm SGS}$ and $C_{\rm SGS}$ are determined by the two square apertures and thin slot, respectively. The equivalent-circuit model for the low-impedance line is two shunt capacitors (C_M).

To obtain the equivalent $L_{\rm SGS} - C_{\rm SGS}$ values of the slotted ground structure, full-wave simulated results are first obtained by using IE3D [8]. Fig. 8 shows the simulated results of the full-wave simulation and the circuit simulation. The circuit simulation is obtained by using AWR Microwave Office. The parameters of the slotted ground structure are $W_1 = 5$ mm, $W_2 = 3.5$ mm, width of thin slot $= 0.2$ mm, and length of thin slot $= 3.5$ mm. The substrate is a 20-mil RT/Duroid 5880 substrate with a dielectric constant of 2.2. Given the required *L–C* values, one can calculate the equivalent $L_{\rm SGS}$ and $C_{\rm SGS}$ by using [7]

$$X_{L_{\rm Required}C_{\rm Required}} = \frac{L_{\rm Required}/C_{\rm Required}}{(\omega_c C_{\rm Required})^{-1} - \omega_c L_{\rm Required}} \tag{4a}$$

$$C_{\rm SGS} = \left(\omega_0 X_{L_{\rm Required}C_{\rm Required}}\left(\frac{\omega_0}{\omega_c} - \frac{\omega_c}{\omega_0}\right)\right)^{-1} \quad (4b)$$

$$L_{\rm SGS} = \left(C_{\rm SGS}\omega_0^2\right)^{-1} \quad (4c)$$

where ω_c is the angular cutoff frequency of the low-pass filter and ω_0 is the resonant angular frequency of the slotted ground structure. When the cutoff frequency $=$ 2 GHz, and the resonant frequency $=$ 6.8 GHz by observing Fig. 8, $C_{\rm SGS} = 0.13$ pF and $L_{\rm SGS} = 4.2$ nH. As shown in Fig. 8, the circuit's simulated results using the above circuit element values show a good agreement with the full-wave simulated results.

The slotted ground structure is then used to build an elliptic-function low-pass filter. From the elliptic-function low-pass prototype filter tables, the element values for $n = 3$, passband ripple $L_{Ar} = 0.1$ dB, and stopband attenuation $L_{As} = 35$ dB with the equal-ripple stopband starting normalized frequency $\Omega_s = 2.921$ are $g_1 = 0.958$, $g_2 = 1.057$, $g_2' = 0.0837$, and $g_3 = 0.958$. Similar to (3), for the cutoff frequency $f_c = 2$ GHz, the required *L–C* values can be calculated with

$$L_{\rm Required} = \frac{Z_0 g_2}{2\pi f_c} = 4.2 \text{ nH} \quad (5a)$$

$$C_{\rm Required} = \frac{g_2'}{Z_0 \times 2\pi f_c} = 0.13 \text{ pF} \quad (5b)$$

$$C_{M,\rm Required} = \frac{g_1}{Z_0 \times 2\pi f_c} = 1.52 \text{ pF}. \quad (5c)$$

Therefore, the slotted ground structure with $W_1 = 5$ mm, $W_2 = 3.5$ mm, width of thin slot $= 0.2$ mm, and length of thin slot $= 3.5$ mm on a 20-mil RT/Duroid 5880 substrate could be readily used. The length of the low-impedance line of $W_2 = 3.5$ mm for C_M can be found from [9]

$$l_2 = \frac{\lambda_g}{2\pi}\sin^{-1}(\omega_c C_M Z_0) \quad (6)$$

where Z_0 is 27.7 Ω for the low-impedance microstrip line and $\lambda_g = 106.5$ mm at the cutoff frequency of 2 GHz. Hence, $l_2 = 9.5$ mm.

Fig. 9 shows the simulated and measured results for the elliptic-function low-pass filter. The full-wave simulation is obtained with IE3D [8], and the required *L–C* values simulation is obtained with AWR Microwave Office. The measured results show a good agreement with the full-wave simulated results. There are some minor discrepancies observed due to fabrication tolerances. From dc to 1.8 GHz, the return loss is better than 15 dB and the insertion loss is less than 0.5 dB. There is one attenuation pole located at 6.4 GHz.

IV. Discussions and Comparisons

The above two filters are discussed and compared here. The filter using distributed elements discussed in Section II is referred to as filter #1, and the filter using a slotted ground structure described in Section III is referred to as filter #2 for simplicity.

1) Fabrication: Since filter #2 uses a slotted ground structure, a double-side etching is required. Therefore, an accurate alignment is required and repeatability might be difficult to maintain for filter #2. On the other hand, filter #1 only requires a one-side etching and is easier to fabricate.
2) Design method: For filter #1, $C_{ps} = C_s + C_p$. Since C_s and C_p are dependent on the selecting of L_s and C_g, respectively, there is less freedom in choosing C_{ps} after L_s and C_g are determined. Therefore, approximation and a time-consuming iteration process are needed. On the other hand, for filter #2, C_M is independent of $L_{\rm SGS}$ and $C_{\rm SGS}$. The design procedure is direct and easier.
3) Integration: Since filter #2 uses a slotted ground structure, tackling the radiation loss problem [7] and the requirement of a special fixture to prevent shorting the slotted ground structure could make it inconvenient to integrate with other components.

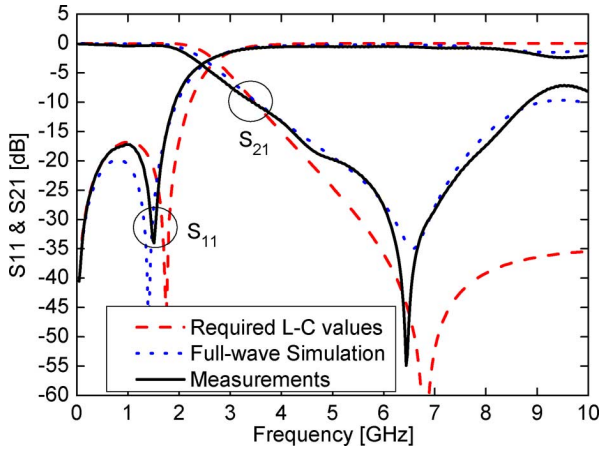

Fig. 9. Simulated and measured results of low-pass filter using slotted ground structure.

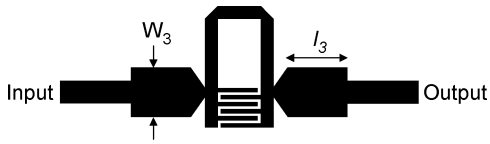

Fig. 10. Schematic of the low-pass filter for comparison. $W_3 = 3.5$ mm, $l_3 = 4.2$ mm [refer to Fig. 4(a)], $l_s = 12.8$ mm, $W_s = 0.9$ mm, $W_c = 0.3$ mm, $G_c = 0.2$ mm, $l_c = 2.8$ mm, and $W_c' = 0.9$ mm.

To further compare these two filters, filter #1 is fabricated on the same 20-mil RT/Duroid 5880 substrate and with the same specifications of filter #2 in Section III ($n = 3$, passband ripple $L_{Ar} = 0.1$ dB, and stopband attenuation $L_{As} = 35$ dB with the equal-ripple stopband starting normalized frequency $\Omega_s = 2.921$). By using the design procedure in Section II, Fig. 10 shows the design schematic and parameters of filter #1. In this case, it should be noted that the sum of C_s and C_p is less than the required C_{ps}, and two low-impedance lines (W_3, l_3) are used to introduce a bigger shunt capacitance. Fig. 11 shows the measured results of these two filters with the following observations.

1) Insertion loss: As shown in Fig. 11(b), filter #2 has a smaller insertion loss than filter #1 by 0.1 dB (average).
2) Circuit size: The circuit size of filter #1 is 15.2×8.6 mm^2, and the circuit size of filter #2 is 24×13.5 mm^2. Filter #1 shows a 60% size reduction in comparison with filter #2.
3) Stopband rejection: Filter #2 shows a better stopband rejection than filter #1. Filter #2 shows not only a better rejection level, but also a wider stopband bandwidth.

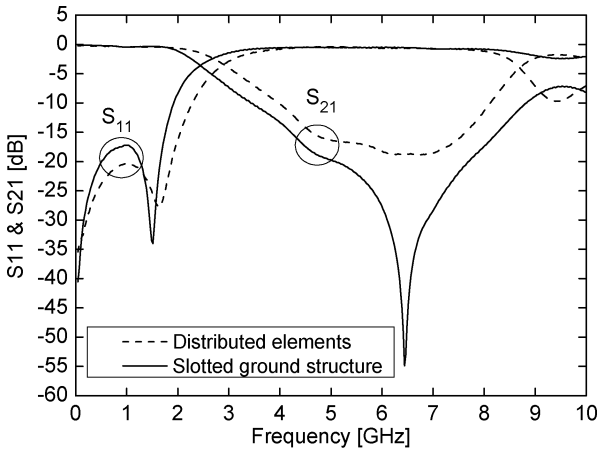

(a)

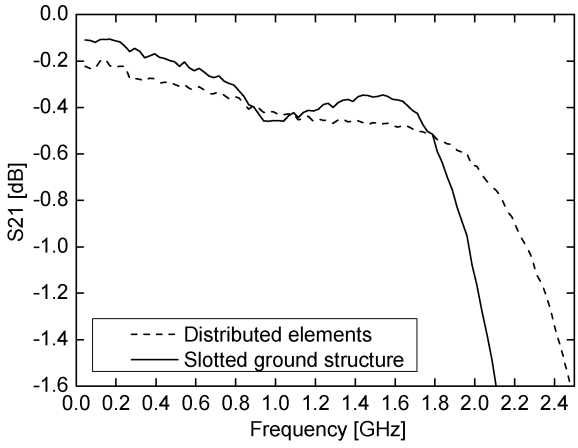

(b)

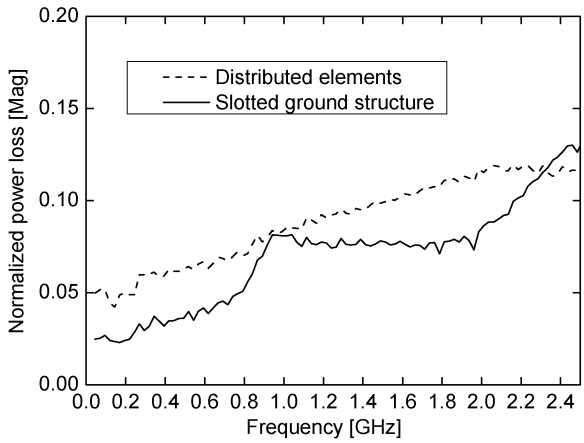

(c)

Fig. 11. Measured results of low-pass filters using distributed elements (filter #1) or slotted ground structure (filter #2). (a) Whole frequency range. (b) Enlarged view within passband. (c) Normalized power loss within passband.

4) Power loss: As shown in Fig. 11(c), the power loss of filter #1 is higher than that of filter #2, where power loss is given as $(1 - |S_{11}|^2 - |S_{21}|^2)$. This might be due to the additional discontinuities introduced by the interdigital capacitor. High power loss might cause unwanted crosstalk in high-density circuits.

V. Conclusions

The design of the microstrip elliptic-function low-pass filters using distributed elements or slotted ground structure has been investigated. With the aid of transmission-line model calculation and full-wave simulation, the equivalent *L–C* values for the low-pass filters have been derived. The measured results show good agreement with the full-wave simulated results. Discussions and comparison of these two filters are also given. These filters should find many applications in microwave/millimeter-wave systems.

Acknowledgment

The authors would like to thank M. Li, Texas A&M University, College Station, for his technical assistance. The authors would also like to thank B. Lewis, Texas A&M University, for reviewing this paper.

References

[1] D. M. Pozar, *Microwave Engineering*. New York: Wiley, 1998, ch. 8.
[2] J.-W. Sheen, "A compact semi-lumped low-pass filter for harmonics and spurious suppression," *IEEE Microw. Wireless Compon. Lett.*, vol. 10, no. 3, pp. 92–93, Mar. 2000.
[3] Y.-W. Lee, S.-M. Cho, G.-Y. Kim, J.-S. Park, D. Ahn, and J.-B. Lim, "A design of the harmonic rejection coupled line low-pass filter with attenuation poles," in *IEEE MTT-S Int. Microw. Symp. Dig.*, 1999, pp. 682–685.
[4] L.-H. Hsieh and K. Chang, "Compact elliptic-function low-pass filters using microstrip stepped-impedance hairpin resonators," *IEEE Trans. Microw. Theory Tech.*, vol. 51, no. 1, pp. 193–199, Jan. 2003.
[5] W.-H. Tu and K. Chang, "Compact microstrip low-pass filter with sharp rejection," *IEEE Microw. Wireless Compon. Lett.*, vol. 15, no. 6, pp. 404–406, Jun. 2005.
[6] D. Ahn, J. S. Park, C. S. Kim, J. Kim, Y. Qian, and T. Itoh, "A design of the low-pass filter using the novel microstrip defected ground structure," *IEEE Trans. Microw. Theory Tech.*, vol. 49, no. 1, pp. 86–93, Jan. 2001.
[7] J. S. Lim, C. S. Kim, D. Ahn, Y. C. Jeong, and S. Nam, "Design of low-pass filters using defected ground structure," *IEEE Trans. Microw. Theory Tech.*, vol. 53, no. 8, pp. 2539–2545, Aug. 2005.
[8] IE3D. ver. 10.2, Zeland Software Inc., Fremont, CA, Dec. 2004.
[9] J.-S. Hong and M. J. Lancaster, *Microstrip Filters for RF/Microwave Applications*. New York: Wiley, 2001.
[10] G. Gonzales, *Microwave Transistors Amplifiers Analysis and Design*. Englewood Cliffs, NJ: Prentice-Hall, 1996, ch. 1.
[11] B. T. Tan, J. J. Yu, S. T. Chew, M.-S. Leong, and B.-L. Ooi, "A miniaturized dual-mode ring bandpass filter with a new perturbation," *IEEE Trans. Microw. Theory Tech.*, vol. 53, no. 1, pp. 343–348, Jan. 2005.

Wen-Hua Tu (S'04) received the B.S. degree in communication engineering from National Chiao Tung University, Hsinchu, Taiwan, R.O.C., in 1999, the M.S. degree in communication engineering from National Taiwan University, Taipei, Taiwan, R.O.C., in 2001, and is currently working toward the Ph.D. degree in electrical engineering at Texas A&M University, College Station.

Since 2003, he has been a Research Assistant with the Electromagnetics and Microwave Laboratory, Texas A&M University, where his research interests include phased-array antennas and microwave devices and circuits.

Kai Chang (S'75–M'76–SM'85–F'91) received the B.S.E.E. degree from National Taiwan University, Taipei, Taiwan, R.O.C., in 1970, the M.S. degree from the State University of New York at Stony Brook, in 1972, and the Ph.D. degree from The University of Michigan at Ann Arbor, in 1976.

From 1972 to 1976, he was a Research Assistant with the Microwave Solid-State Circuits Group, Cooley Electronics Laboratory, The University of Michigan at Ann Arbor. From 1976 to 1978, he was with Shared Applications Inc., Ann Arbor, MI, where he was involved with computer simulation of microwave circuits and microwave tubes. From 1978 to 1981, he was with the Electron Dynamics Division, Hughes Aircraft Company, Torrance, CA, where he was involved in the research and development of millimeter-wave solid-state devices and circuits, power combiners, oscillators, and transmitters. From 1981 to 1985, he was with TRW Electronics and Defense, Redondo Beach, CA, as a Section Head, where he developed state-of-the-art millimeter-wave integrated circuits and subsystems including mixers, voltage-controlled oscillators (VCOs), transmitters, amplifiers, modulators, upconverters, switches, multipliers, receivers, and transceivers. In August 1985, he joined the Electrical Engineering Department, Texas A&M University, College Station, as an Associate Professor and became a Professor in 1988. In January 1990, he was appointed Raytheon E-Systems Endowed Professor of Electrical Engineering. He has authored and coauthored several books, including *Microwave Solid-State Circuits and Applications* (Wiley, 1994), *Microwave Ring Circuits and Antennas* (Wiley, 1996; 2nd ed., 2004), *Integrated Active Antennas and Spatial Power Combining* (Wiley, 1996), *RF and Microwave Wireless Systems* (Wiley, 2000), and *RF and Microwave Circuit and Component Design for Wireless Systems* (Wiley, 2002). He has served as the Editor of the four-volume *Handbook of Microwave and Optical Components* (Wiley, 1989 and 1990; 2nd ed., 2003). He is the Editor of *Microwave and Optical Technology Letters* and the Wiley Book Series on "Microwave and Optical Engineering" (over 70 books published). He has authored or coauthored over 450 papers and numerous book chapters in the areas of microwave and millimeter-wave devices, circuits, and antennas. He has graduated over 25 Ph.D. students and over 35 M.S. students. His current interests are microwave and millimeter-wave devices and circuits, microwave integrated circuits, integrated antennas, wideband and active antennas, phased arrays, microwave power transmission, and microwave optical interactions.

Dr. Chang has served as technical committee member and session chair for the IEEE Microwave Theory and Techniques Society (IEEE MTT-S), the IEEE Antennas and Propagation Society (IEEE AP-S), and numerous international conferences. He was the vice general chair for the 2002 IEEE International Symposium on Antennas and Propagation. He was the recipient of the 1984 Special Achievement Award presented by TRW, the 1988 Halliburton Professor Award, the 1989 Distinguished Teaching Award, the 1992 Distinguished Research Award, and the 1996 Texas Engineering Experiment Station (TEES) Fellow Award presented by Texas A&M University.